Supporting Online Material for

Polariton Superfluids Reveal Quantum Hydrodynamic Solitons

A. Amo,* S. Pigeon, D. Sanvitto, V. G. Sala, R. Hivet, I. Carusotto, F. Pisanello, G. Lemenager, R. Houdré, E Giacobino, C. Ciuti, A. Bramati*

*To whom correspondence should be addressed. E-mail: alberto.amo@lpn.cnrs.fr (A.A.); bramati@spectro.jussieu.fr (A.B.)

Published 3 June 2011, *Science* **332**, 1167 (2011)
DOI: 10.1126/science.1202307

This PDF file includes:

Materials and Methods
Figs. S1 to S4

Polariton superfluids reveal quantum hydrodynamic solitons

A. Amo[1,2], S. Pigeon[3], D. Sanvitto[4], V. G. Sala[1], R. Hivet[1], I. Carusotto[5], F. Pisanello[1,4], G. Lemenager[1], R. Houdré[6], E Giacobino[1], C. Ciuti[3], A. Bramati[1]

[1]*Laboratoire Kastler Brossel, Université Pierre et Marie Curie-Paris 6, École Normale Supérieure et CNRS, UPMC Case 74, 4 place Jussieu, 75005 Paris, France*
[2]*CNRS-Laboratoire de Photonique et Nanostructures, Route de Nozay, 91460 Marcoussis, France*
[3]*Laboratoire Matériaux et Phénomènes Quantiques, UMR 7162, Université Paris Diderot-Paris 7 et CNRS, 75013 Paris, France*
[4]*NNL, Istituto Nanoscienze - CNR, Scuola Superiore ISUFI, Università del Salento, Via Arnesano, 73100 Lecce, Italy*
[5]*INO-CNR BEC Center and Dipartimento di Fisica, Università di Trento, via Sommarive 14, I-38123 Povo, Italy*
[6]*Institut de Physique de la Matière Condensée, Faculté des Sciences de Base, bâtiment de Physique, Station 3, EPFL, CH-1015 Lausanne, Switzerland*

Materials and Methods

Sample description

Our sample is a 3λ/2 GaAs cavity with three $In_{0.05}Ga_{0.95}As$ quantum wells resulting in a Rabi splitting of 5.1 meV, and a polariton lifetime of about 15 ps. The top/bottom distributed Bragg reflectors forming the cavity have 21/24 pairs of GaAs/AlGaAs alternating layers with an optical thickness of λ/4, λ being the wavelength of the energy of the confined cavity mode. All our experiments are performed at zero exciton-cavity detuning, with a continuous wave single mode laser quasi-resonant with the lower polariton branch.

The sample has been grown by molecular beam epitaxy. During the growth of the distributed Bragg reflectors, the slight lattice mismatch between the materials of each layer results in an accumulated stress which relaxes in the form of structural defects. These photonic defects form a very high potential barrier in the polariton energy landscape.

Confocal excitation scheme

The data reported in Fig. 3 have been taken making use of the confocal excitation scheme represented in Fig. S1. The laser is focalised in an intermediate plane where a mask is placed in order to hide the upper part of the Gaussian spot on that plane. Then, an image of the intermediate plane is done on the sample, producing a spot with the shape of a half Gaussian (the profile is depicted in the inset of Fig. S1). Polaritons are resonantly injected in the microcavity with a well defined wavevector, in the region above the red line in the figure. In these conditions, polaritons move out of the excitation spot with a free phase, not imposed by the pump beam. This is essential for the observation of hydrodynamic effects involving topological excitations with phase discontinuities.

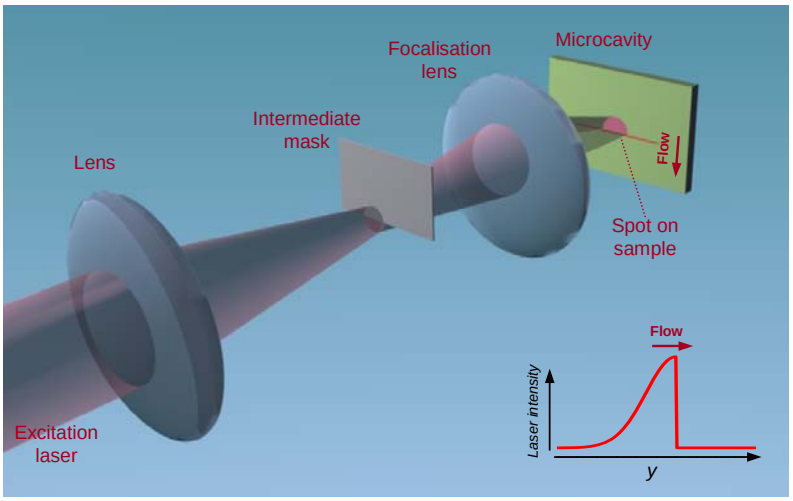

Fig. S1. Excitation setup used for the experiments reported in Fig. 3. The intermediate mask creates a spot on the sample with the shape of a half Gaussian (the inset shows a *y* cross-section of the spot).

Estimation of the sound speed

The average sound speeds reported in the main manuscript have been obtained from the measured soliton speed v_s and phase jump δ, with the use of Eq. 1 ($\cos(\delta/2) = v_s/c_s$). In Figs. 1 and 3 we have estimated the sound speed in the soliton regime (Fig. 1a, 1c and Fig. 3c, 3f) in the region below the potential barrier, where the hydrodynamic effects are observed. We have taken as the soliton speed $v_s = v_{flow} \sin\alpha$, where 2α is the angle of aperture of the soliton pair, and v_{flow} is obtained from the injected polariton wavevector and the measured polariton mass via $v_{flow} = k\hbar/m_{pol}$.

In the case of Fig. 3, the sound speed is estimated from the phase jump at half the total propagation distance in the soliton regime (Fig. 3c, 3f). In order to obtain the sound speed for other two excitation densities (panels a,b,d,e,g,h), we use the measured polariton density relative to the soliton case (c,f) and the sound speed relation $c_s = \sqrt{\hbar g |\psi|^2 / m_{pol}}$. Note that the sound speed is proportional to the square root of the density $|\psi|^2$.

In order to confirm that this relationship is consistent with our results, we proceed in the same way for the data plotted in fig. 1. In this case we take the sound speed obtained from the phase jump along the right soliton. The sound speed decays as the fluid is further away from the excitation area. The result is shown in black dots in Fig. S2. Additionally, we measure the decay of the density on the edges of the soliton along the soliton line. In Fig. S2 we plot in green triangles the magnitude $c_s = A\sqrt{I}$, where I is the emitted intensity (proportional to the polariton density) and A is a fitting constant. The figure shows that the decay of the sound speed obtained from both the phase jump and the measured density follow the same trend.

These results justify our method to obtain the sound speed in the superfluid and vortex emission regimes (Fig. 3a,b) from the measured sound speed in the soliton regime (Fig. 3c, obtained from the phase jump) and the relative polariton density.

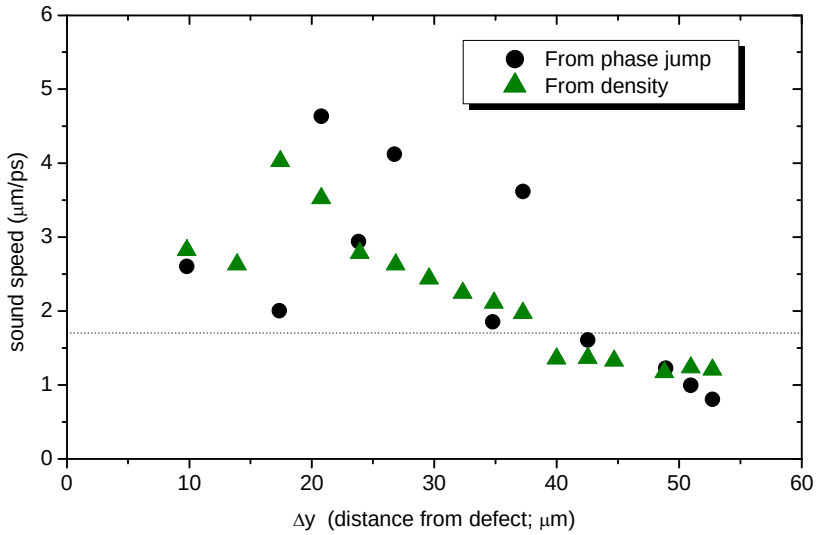

Fig. S2. Sound speed estimation for the data of Fig. 1. Black dots show the sound speed obtained from the phase jump and Eq. 1 along the soliton trajectory. Green triangles show the fit from the measured square root of the emitted intensity (proportional to the polariton density). The dashed line shows the fluid speed.

Degree of first order coherence

The degree of first order coherence, $g^{(1)}$, is defined as:

$$g^{(1)}(\boldsymbol{r_1},\boldsymbol{r_2},t,\tau)=\frac{\left\langle \psi^{\dagger}(\boldsymbol{r_1},t)\psi(\boldsymbol{r_2},t+\tau)\right\rangle}{\sqrt{\left\langle \left|\psi(\boldsymbol{r_1},t)\right|^2\right\rangle\left\langle \left|\psi(\boldsymbol{r_2},t+\tau)\right|^2\right\rangle}}.$$

In our cw experiments in stationary conditions, $g^{(1)}$ is independent of t. In order to measure $g^{(1)}$ (τ=0), we direct the emitted light from the polariton condensate, which contains all the coherence information of the wavefunction, into a modified Mach-Zehnder interferometer. The interference image is obtained from the composition of the real space emitted field with coordinate $\boldsymbol{r_1}$, and a reference beam issued from the enlarging of a small area of the emission with a fixed position $\boldsymbol{r_2}$ with a well defined spatial phase. By varying the length of the reference beam arm by up to two wavelengths around zero delay, we measure the visibility of the fringes of the interferometric image, giving direct access to the time averaged real space degree of coherence of the condensate wavefunction $\psi(\boldsymbol{r_1},t)$ with respect to a coherent reference $\psi(\boldsymbol{r_2},t)$.

Gross-Piteavskii equation

Figure 2 shows simulations based on the solution of a generalized non-equilibrium Gross-Pitaevskii equation describing the polariton condensate subject to interparticle interactions. In the basis of the confined exciton and photon wavefunctions it has the form:

$$i\frac{d}{dt}\begin{pmatrix}\psi_C(\mathbf{x},t)\\ \psi_X(\mathbf{x},t)\end{pmatrix}=\begin{pmatrix}F_p e^{i(\mathbf{k}_p\mathbf{x}-\omega_p t)}\\ 0\end{pmatrix}e^{-\frac{(\mathbf{x}-\mathbf{x}_0)^2}{2\delta_{\mathbf{x}}^2}}+$$
$$\left[\mathbf{h}^0+\begin{pmatrix}V_C(\mathbf{x})-i\frac{\gamma_C}{2} & 0\\ 0 & -i\frac{\gamma_X}{2}+g|\psi_X(\mathbf{x},t)|^2\end{pmatrix}\right]\begin{pmatrix}\psi_C(\mathbf{x},t)\\ \psi_X(\mathbf{x},t)\end{pmatrix},$$

where,

$$\mathbf{h}^0=\begin{pmatrix}\omega_C(-i\nabla) & \Omega_R\\ \Omega_R & \omega_X(-i\nabla)\end{pmatrix},$$

where, $\boldsymbol{x}$ is a two-dimensional spatial vector, $\psi_{X(C)}$ is the exciton (cavity photon) wavefunction, F_p, k_p and $\hbar\omega_p$ are, respectively, the amplitude, momentum and energy of the pump field. The k-dependent energy of the excitons (cavity photons) is described by $\hbar\omega_{X(C)}$, $\gamma_{X(C)}$ is the decay rate of the excitons (cavity photons), with a value of 16 ps, $2\hbar\Omega_R$ is the vacuum Rabi splitting between the polariton modes (5.1 meV), $V_C(\boldsymbol{x})$ is the photonic potential barrier, g the exciton-exciton interaction constant, taken to be 0.01 meV μm^2. $\boldsymbol{x_0}$ indicates the position of the centre of the Gaussian spot on the sample, while δ_X is its radial width. In the simulations shown Fn fig. 2, k_p =0.73 μm^{-1} and the pump energy is detuned from the lower polariton branch at that k_p by 0.2 meV. The defect is simulated as a rectangle of 5x3 μm and a height of 80 meV.

Supporting Figure 3

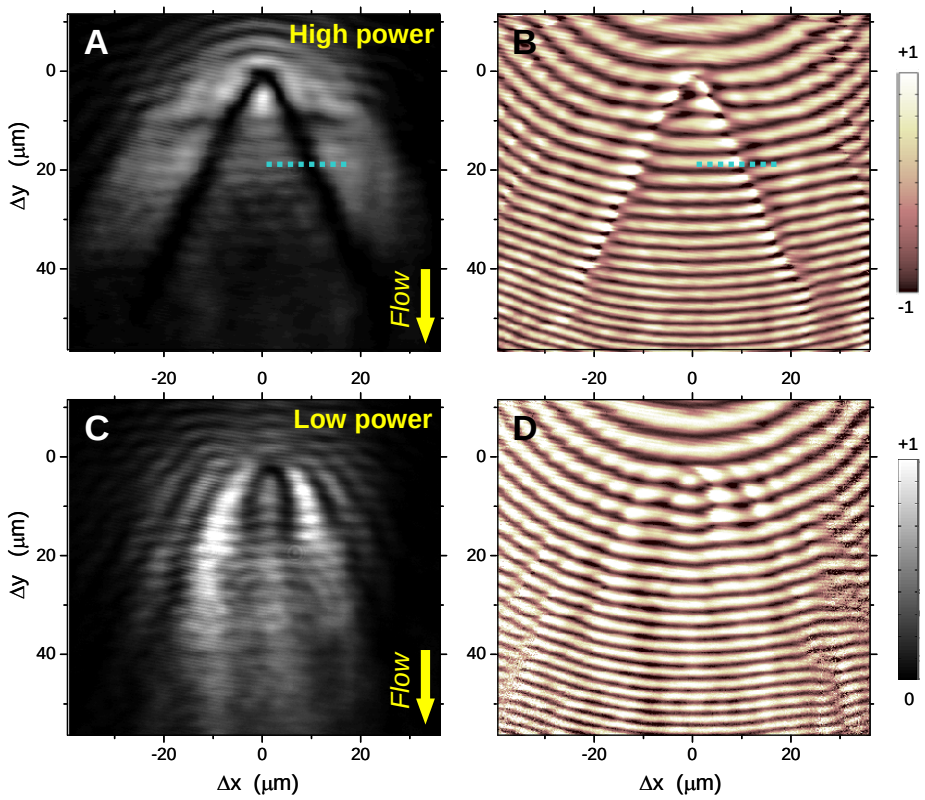

Fig. S3. (**A**) Real space emission showing oblique dark solitons at high excitation density (85 mW), and (**B**) the corresponding interference pattern showing the phase slip along the soliton trajectory (reproduced from Fig. 1A and C). (**C** and **D**) Real space emission and corresponding interference pattern at low excitation density (10 mW). In this case, polariton-polariton interactions are negligible and solitons are neither formed nor sustained in the fluid. The parabolic wave patterns observed in (C) arise from the interference between the injected polaritons and those elastically scattered by the defect. The interference pattern (D) does not show phase jumps as those associated to solitons.

Supporting Figure 4

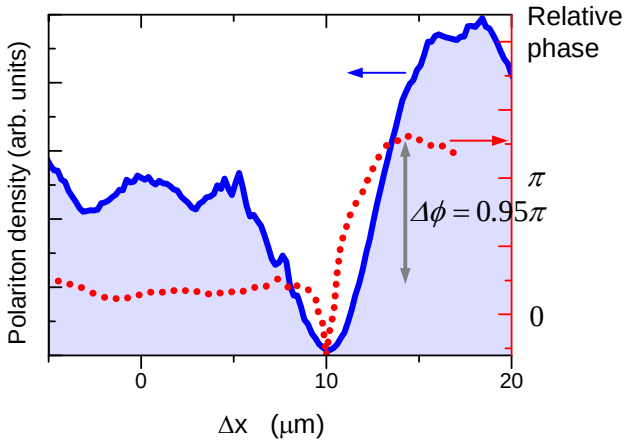

Fig. S4. Intensity (blue line) and phase profile (red dots), along the dashed line indicated in Fig. S3, showing a phase jump of the condensate wavefuntion of almost π across the the soliton.